Article No. jmbi.1998.2452 available online at http://www.idealibrary.com on IDEAL *J. Mol. Biol.* (1999) **285**, 2089–2104

JMB

Structure of Extracellular Tissue Factor Complexed with Factor VIIa Inhibited with a BPTI Mutant

Erli Zhang, Robert St. Charles and A. Tulinsky*

Department of Chemistry
Michigan State University East
Lansing, MI 48824, USA

The event that initiates the extrinsic pathway of blood coagulation is the association of coagulation factor VIIa (VIIa) with its cell-bound receptor, tissue factor (TF), exposed to blood circulation following tissue injury and/or vascular damage. The natural inhibitor of the TF·VIIa complex is the first Kunitz domain of tissue factor pathway inhibitor (TFPI-K1). The structure of TF·VIIa reversibly inhibited with a potent ($K_i = 0.4$ nM) bovine pancreatic trypsin inhibitor (BPTI) mutant (5L15), a homolog of TFPI-K1, has been determined at 2.1 Å resolution. When bound to TF, the four domain VIIa molecule assumes an extended conformation with its light chain wrapping around the framework of the two domain TF cofactor. The 5L15 inhibitor associates with the active site of VIIa similar to trypsin-bound BPTI, but makes several unique interactions near the perimeter of the site that are not observed in the latter. Most of the interactions are polar and involve mutated positions of 5L15. Of the eight rationally engineered mutations distinguishing 5L15 from BPTI, seven are involved in productive interactions stabilizing the enzyme-inhibitor association with four contributing contacts unique to the VIIa·5L15 complex. Two additional unique interactions are due to distinguishing residues in the VIIa sequence: a salt bridge between Arg20 of 5L15 and Asp60 of an insertion loop of VIIa, and a hydrogen bond between Tyr34O of the inhibitor and Lys192NZ of the enzyme. These interactions were used further to model binding of TFPI-K1 to VIIa and TFPI-K2 to factor Xa, the principal activation product of TF·VIIa. The structure of the ternary protein complex identifies the determinants important for binding within and near the active site of VIIa, and provides cogent information for addressing the manner in which substrates of VIIa are bound and hydrolyzed in blood coagulation. It should also provide guidance in structure-aided drug design for the discovery of potent and selective small molecule VIIa inhibitors.

Keywords: multi-domain enzymes; ternary protein complex; tissue factor pathway inhibitor; Kunitz domains

**Corresponding author*

Present address: E. Z. Zhang, Parke-Davis Pharmaceutical Research, 2800 Plymouth Road, Ann Arbor, MI 48105, USA

Abbreviations used: TF, tissue factor; VII, factor VII; VIIa, factor VIIa; IXa, factor IXa; Xa, factor Xa; Gla, γ-carboxyglutamic; EGF, epidermal growth factor; TF·VIIa, tissue factor-factor VIIa complex; IX, factor IX; X, factor X; DFFR, D-Phe-Phe-Arg chloromethyl ketone; TFPI, tissue factor pathway inhibitor; BPTI, bovine pancreatic trypsin inhibitor; TFPI-K1, first Kunitz domain of TFPI; TFPI-K2, second Kunitz domain of TFPI; 5L15, BPTI mutant; TF·VIIa·5L15, TF·VIIa reversibly inactivated at the active site with 5L15; TF·VIIa·DFFR, TF·VIIa irreversibly inactivated at the active site with DFFR; MALDI-MS, matrix-assisted laser desorption ionization mass spectroscopy; TF1, N-terminal TF domain (Thr6**T**-Asn107**T**); TF2, C-terminal TF domain (Leu108**T**-Glu210**T**); VII central, variant of VII; VIIa central, variant of VIIa.

E-mail address of the corresponding author: Tulinsky@cemvax.cem.msu.edu

0022-2836/99/052089–16 $30.00/0

Introduction

The primary components in the initiation of the extrinsic pathway of blood coagulation are tissue factor (TF) and factor VII (VII). The former is a non-enzymic, cell membrane bound glycoprotein cofactor exposed by vascular injury (Nemerson, 1988). The zymogen VII is a multidomain, single chain vitamin K-dependent glycoprotein ($M_r \sim 50$ kDa; Ichinose & Davie, 1994). Binding of TF to VII promotes the activation of VII to the enzyme factor VIIa (VIIa; Rao & Rapaport, 1988). The activation proceeds through limited proteolysis of the Arg152-Ile153 peptide bond and can be accomplished by any of a number of blood serine proteinases, such as factors IXa and Xa (IXa and Xa, respectively), including VIIa (Davie *et al.*, 1991), and takes place optimally in the presence of Ca^{2+} and negatively charged phospholipid. The resultant two chain multi-domain enzyme bridged by a disulfide bond is composed of a light chain N-terminal γ-carboxyglutamic (Gla)-rich Gla domain, followed by two epidermal growth factor modules (EGF1, EGF2) and a heavy chain trypsin-like catalytic domain.

The integral membrane TF molecule consists of a soluble N-terminal extracellular part (1-219), a single membrane spanning region (220-242), and a short 20 residue cytoplasmic C-terminal tail (243-262; Fisher *et al.*, 1987; Morrissey *et al.*, 1987; Spicer *et al.*, 1987; Scarpati *et al.*, 1987). It functions as an essential cofactor for VIIa, dramatically enhancing its catalytic efficiency for macromolecular protein substrates (~10,000-fold; Osterud & Rapaport, 1977; Silverberg *et al.*, 1977). The TF·VIIa complex ($K_d = 0.4$ pM) activates factors IX and X (IX and X, respectively), which ultimately results in thrombin generation and formation of the blood clot. The extracellular domain of TF is related to the cytokine receptor family that is made up of two repeat β-sandwiches containing a three and a four-stranded sheet with fibronectin type III topology (Baron *et al.*, 1992; Leahy *et al.*, 1992). The crystal structure of extracellular TF has been determined independently by three groups (Harlos *et al.*, 1994; Muller *et al.*, 1994, 1996; Huang *et al.*, 1998). The only three-dimensional structure of the TF·VIIa complex that has been determined is with VIIa irreversibly inhibited at the active site with D-Phe-Phe-Arg-chloromethyl ketone (DFFR; Banner *et al.*, 1996).

The endogenous inhibitor of TF·VIIa is tissue factor pathway inhibitor (TFPI), which is multivalent with three tandemly arranged bovine pancreatic trypsin inhibitor (BPTI)-like Kunitz protease inhibitor domains (Rapaport, 1989; Broze *et al.*, 1990). Inhibition of the extrinsic pathway coagulation machinery by TFPI takes place by initial binding to and inhibition of Xa by TFPI Kunitz domain 2 (K2; $K_i = 20$ pM), followed by the binding and inhibition of VIIa of the TF·VIIa complex through TFPI Kunitz domain 1 (*K*1; $K_i = 120$ nM; Petersen *et al.*, 1996). Anticoagulant activity of TFPI is reduced with the proteolytic removal of a C-terminal fragment indicating that other regions of TFPI are involved in its function (Wesselschmidt *et al.*, 1992). This is further supported by the fact that the TFPI-K2 domain alone binds with considerably reduced affinity with Xa (90 nM) and even less with the TF·VIIa complex, while a separate TFPI-K1 domain does not bind to Xa at all and with only half the affinity of TFPI for the TF·VIIa complex (Wesselschmidt *et al.*, 1992; Petersen *et al.*, 1992, 1996; Higuchi *et al.*, 1992). The third Kunitz domain does not bind to either enzyme by itself.

The Kunitz-type proteinase inhibitor BPTI, specific for trypsin ($K_i = 10$-15 pM), has been intensively studied over the years, and has even been used in humans as an antithrombotic drug in cardiac surgery (Verstraete, 1985; Hardy & Desroches, 1992). Based on the three-dimensional structure of BPTI complexed with trypsin (Huber *et al.*, 1974) and its homology with the Kunitz domains of TFPI (Figure 1), a group of BPTI mutant inhibitors for coagulation enzymes with activities in the nanomolar range was constructed by recombinant methods (Ripka *et al.*, 1995; Stassen *et al.*, 1995). Selected residues of BPTI in its contact region with trypsin were mutated: some were directed active site mutations in the P5-P4′ binding region of the inhibitor, while the remainder were at other trypsin contact residues. The mutations were optimized by random mutagenesis using phage display technology for selection (Stassen *et al.*, 1995). Two of the mutant inhibitors resulting from the survey have inhibition constants for TF·VIIa of less than 1 nM and another is 5 nM. One of these, 5L15

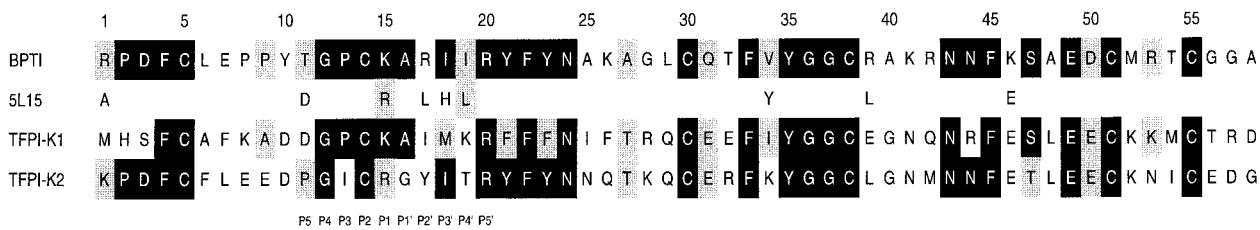

Figure 1. Kunitz domain sequences. Only mutations of 5L15 with respect to BPTI are shown; the alanine mutation at the N-terminal is for expression purposes only. Black and shaded residues conserved and homologous, respectively, with respect to BPTI. The P5-P5′ inhibitor binding sites are indicated.

(Figure 1), with a total of eight mutations, is not only highly potent for the TF·VIIa complex ($K_i = 0.4$ nM), but also fairly selective with respect to other coagulation enzymes (Stassen *et al*., 1995). Of the eight mutations, only two were homologous (Figure 1), two produced the same amino acid residue as in TFPI-K1 (Asp11, Asp46) while one of the former (Lys15Arg) appeared to be a superior replacement at the P1 specificity position. In the absence of the VIIa·5L15 bound structure, nothing more was certain from the mutations.

Two different trigonal crystal forms of the TF·VIIa·5L15 complex belonging to space group $P32_1$ have been reported (Stura *et al*., 1996). One of the forms only diffracts X-rays to 7.0 Å resolution, while the other is better, diffracting to about 3.2 Å resolution. The crystallographic work, however, was hampered because only 1.5 mg of the complex was available for crystallization (Stura *et al*., 1996). Although X-ray intensity data were collected from each of the forms, the structure of this ternary complex remains undetermined. We have also succeeded in crystallizing 5L15 inhibited VIIa complexed with TF, but under different conditions producing a different crystalline arrangement (orthorhombic, space group $C222_1$) that diffracts X-rays at 2.1 Å resolution. Here, we present the refined structure of the TF·VIIa·5L15 ternary complex, and we compare it with the structure of the irreversibly inhibited TF·VIIa·DFFR complex and that of the binary BPTI·trypsin complex. In addition, respective models for the structures of the first two Kunitz domains of TFPI interacting with VIIa and Xa are presented based on the structure of 5L15 and VIIa·5L15 interactions, and the multi-domain structure of VIIa is compared with the intact multidomain structure of IXa.

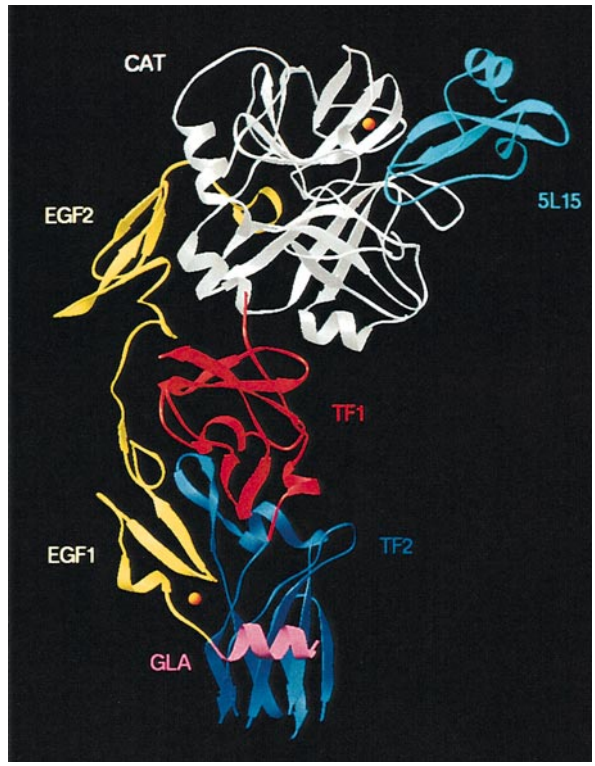

Figure 2. Ribbon drawing of TF·VIIa·5L15 complex. The various domains labeled in same color as the domains (see the text for abbreviations); the Ca^{2+} are shown as orange-yellow spheres.

Results and Discussion

The overall structure of the TF·VIIa·5L15 complex has an extended conformation approximately 106 Å long with a diameter varying between 40-60 Å. This is shorter than TF·VIIa·DFFR (Banner *et al*., 1996), because there is only electron density for the C-terminal helix of the Gla domain in TF·VIIa·5L15 (Figure 2). This led to the measurement of the matrix-assisted laser desorption ionization mass spectrum (MALDI-MS) of VIIa, which was compared with that of a crystal. The VIIa of crystalline material was about 4.2 kDa less than the VIIa used to form the complex, which corresponds closely with the N-terminal 32 residues, so it was concluded that VIIa in the crystalline complex lacked most of the Gla domain. The gross topology of the complex, however, is similar to the DFFR inhibited complex, but differs somewhat around the active site region, where the latter possesses only a bound tripeptide methyl ketone compared with the 58 folded residues of the 5L15 inhibitor. There is also a difference in the position of the C-terminal helix of the Gla domain. Several segments of the TF·VIIa·5L15 structure are incomplete due to poor or missing electron density. This includes most notably the N-terminal two-thirds or so of the Gla domain, about ten C-terminal residues of the light chain of VIIa, a tripeptide loop of the catalytic domain, and parts of a few solvent-accessible loops in the C-terminal domain of TF (TF2 of Figure 2) that abut or embed into membrane in the physiological complex. Some of these features were also missing in the TF·VIIa·DFFR structure (last ten residues of VIIa light chain) and even in the apo-structures of soluble TF (membrane proximal loops). The VIIa molecule is bound to TF through many interactions with regions of both the light and heavy chains of VIIa. The VIIa interaction surface of TF extends most of the length of the two domain TF molecule, which forms a rigid scaffold-like support upon which the individual VIIa structural modules are bound. The 5L15 mutant inhibitor binds at the active site of VIIa in a non-covalent way, with its principal ellipsoidal axis oriented roughly perpendicular with the surface of the catalytic domain (Figure 2), similar to that observed for BPTI in the trypsin-BPTI complex (Huber *et al*., 1974), and it makes numerous interactions with the active site of VIIa and surrounding environment.

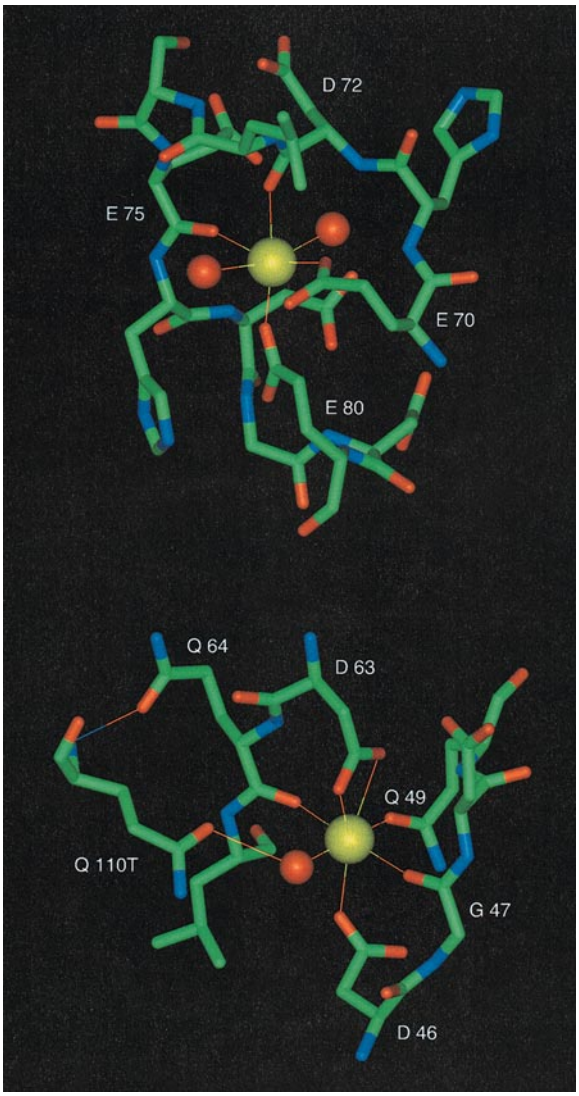

Figure 3. High-affinity calcium binding sites of VIIa. Catalytic domain, top (chymotrypinogen numbering); EGF1-Gla interface, bottom (sequential numbering). Calcium, yellow sphere; water, red spheres; VIIa residues in atom colors (carbon, green; nitrogen, blue; oxygen, red).

The catalytic domain of VIIa

To differentiate between the residues in different molecules of the ternary complex and to conform with the numbering scheme adopted previously for the TF·VIIa·DFFR complex (Banner *et al.*, 1996), a bold chain identifier will follow each residue number (except for 5L15): **T** for TF, **L** for VIIa light chain and **H** for VIIa heavy chain. Sequential numbering described for TF (Harlos *et al.*, 1994) and VIIa (Ichinose & Davie, 1994) will be used. Standard chymotrypsinogen numbering for serine proteases (Bode *et al.*, 1992) will additionally be given in curly brackets for the catalytic domain of VIIa, which may also have an alphabetic insertion code.

Table 1. Calcium coordination distances of the high-affinity binding sites of TF·VIIa·5L15

Catalytic domain Ligand	*d* (Å)	Gla-EGF1 site Ligand	*d* (Å)
Glu210**H**:OE1{70}	2.51	Asp46**L**:OD2	2.93
Asp212**H**:O{72}	2.43	Gly47**L**:O	2.20
Glu215**H**:O{75}	2.11	Asp63**L**:OD1	2.76
Glu220**H**:OE2{80}	2.22	Asp63**L**:OD2	2.22
O^w139	2.38	Gln64**L**:O	2.55
O^w167	3.01	Gln49**L**:OE1	2.48
		O^w455	1.97

The structure of the catalytic domain is complete except for a tripeptide adjacent to an insertion bordering the active site (Val317**H**-Asp319**H**){170E-172}. Otherwise, the catalytic domain and active site region of VIIa are well defined in electron density. Based on a superposition of C^α-coordinates, the folding of the catalytic domain and EGF2 of 5L15-inhibited VIIa is very similar to that of the DFFR complex: the rms difference in 233 optimally superposed C^α-positions between the catalytic domains is only 0.35 Å, while the same applies to the two EGF2 domains. A similar comparison of equivalent residues of trypsin in the trypsin·BPTI complex and the catalytic domain of VIIa gives a rms difference of 0.70 Å.

The zymogen and VIIa possess two high-affinity calcium binding sites (Strickland & Castellino, 1990; Figure 2). The catalytic domain has one of these sites ($K_d \sim$ 100-200 μM; Sabharwal *et al.*, 1995), similar to those found in IX (Bajaj *et al.*, 1992) and X (Persson *et al.*, 1993). Based on the structure of trypsin (Bode & Schwager, 1975), which also contains a calcium binding site, the residues forming the site in VIIa were predicted (Bajaj *et al.*, 1992). These are confirmed by the structures of TF·VIIa·5L15 and TF·VIIa·DFFR. The site can be described as a slightly distorted octahedral arrangement around a Ca^{2+} with two apical water molecules (O^w139, O^w167) and an equatorial plane consisting of: Glu210**H**:OE1{70}, Asp212**H**:O{72}, Glu215**H**:O{75}, Glu220**H**:OE2{80} (Figure 3). The apical positions are further connected to two clusters of solvent-exposed water molecules that form an extended hydrogen-bonding network on either side of the Ca^{2+} binding loop (Glu210**H**-Gln220**H**){70-80}, which is itself a surface feature. The site in TF·VIIa·5L15 differs a little from that of TF·VIIa·DFFR where Asp217**H**{77} is said to bind to the calcium through a water molecule.

The K_d of TF·VIIa is about 1.5 μM in the absence of Ca^{2+} (Sabharwal *et al.*, 1995), whereas it is 0.4 pM in their presence. The difference of 10^6 in binding (about 8 kcal mol^{-1}) is difficult to reconcile based solely on the catalytic domain Ca^{2+} site. The Ca^{2+} site of the catalytic domain is on the surface of VIIa, far from TF (~18 Å; Figure 2), with which it does not interact directly. The difference in binding must, therefore, be the result of a cumulative effect involving the other high-affinity site of VIIa and interactions that take place between TF and a

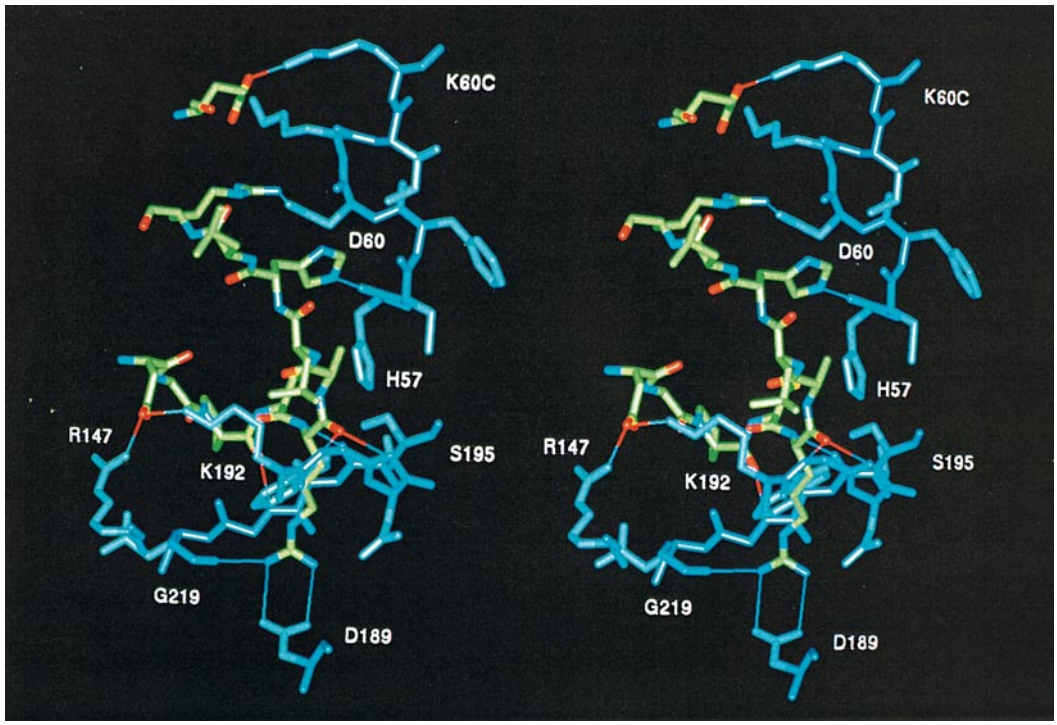

Figure 4. Stereoview of most of the polar interactions of 5L15 with VIIa. The 5L15 residues Asp11-Arg20 and Glu46 in atom colors, VIIa residues in blue; pertinent VIIa residues in chymotrypsinogen numbering. The hydrogen bonds are dual colored thin lines.

Ca^{2+}-mediated (folded) Gla domain structure. The refined occupancy of the Ca^{2+} in the catalytic domain of TF·VIIa·5L15 is 0.8 with a *B*-factor of 24 Å^2. The Ca^{2+}-oxygen distances of the catalytic site are given in Table 1, in general agreement with the Ca^{2+} site of trypsin.

Thrombin binds sodium and other monovalent cations (Orthner & Kosow, 1980), as does Xa (Orthner & Kosow, 1978) and protein C (Steiner & Castellino, 1982), and the binding has been shown to produce allosteric effects in these enzymes (Wells & DiCera, 1992). The Na^+ binding region of thrombin (Zhang & Tulinsky, 1997) has been compared here with the homologous region of the catalytic domain of TF·VIIa·5L15, which shows no indications of Na^+ binding. Superposing the catalytic domain of VIIa with thrombin (rms$\Delta = 1.0$ Å, 212 C^α atom pairs) shows that the carbonyl oxygen atoms of Thr370**H**{221A} and His373**H**{224} are close to those of Arg221AO and Lys224O of thrombin that coordinate directly to the Na^+ along with four water molecules in an octahedral array. However, the shorter heptapeptide (Gly331**H**-Lys337**H**){184-188} loop of VIIa, stacking closely upon the hexapeptide (Ile323**H**-Phe328**H**){176-181} loop, homologous and isostructural with thrombin, occupies the space of the Na^+ coordinating water molecules and surrounding solvent in thrombin. The loop is a more extensive decapeptide in thrombin that is open and accessible to Na^+ coordinating water molecules and bulk solvent (Zhang & Tulinsky, 1997). It thus appears that the critical factor hindering Na^+ binding in VIIa is the tight (Gly331**H**-Lys337){184-188} surface loop.

The 5L15 structure

As expected, considering that only eight residues of BPTI are different, the main-chain folding of 5L15 is practically the same as that of BPTI in the trypsin·BPTI complex (rms$\Delta = 0.35$ Å). Electron density for the 5L15 molecule is generally of good quality, except for the far distal part of the inhibitor (furthest from the active site of VIIa). There the density is weaker, with some breaks, particularly near the C-terminal helix, where the atoms in the region have correspondingly larger temperature factors ($B \sim 48$ Å^2 compared with $\langle B \rangle = 35$ Å^2 for 5L15). The 5L15 mutations did not produce any new intramolecular polar interactions with respect to BPTI. The effect of the mutations on hydrophobicity was more difficult to gauge with nothing strikingly obvious.

The VIIa·5L15 interactions

The 5L15 mutant binds to the active site of VIIa like trypsin-bound BPTI (Huber *et al.*, 1974). The rmsΔ of the C^α positions between VIIa·5L15 and trypsin·BPTI is 1.0 Å. The primary binding loop of the inhibitor (Asp11-Leu19), which makes an antiparallel β-strand interaction with VIIa and mimicks substrate binding, interacts directly and extensively with the active site S5-S4′ binding subsites

Table 2. Polar interactions of VIIa·5L15

5L15	VIIa	*d* (Å)	
Asp11OD2	Arg290**H**:NH1{147}	2.63	Salt bridge
Asp11OD2	Lys341**H**:NZ{192}	2.65	Salt bridge
Pro13O	Gly365**H**:N{216}	2.97	
Arg15N	Ser344**H**:OG{195}	3.12	
Arg15N	Ser363**H**:O{214}	3.44	
Arg15NH1	Asp338**H**:OD1{189}	3.07	Salt bridge
Arg15NH2	Asp338**H**:OD2{189}	3.10	Salt bridge
Arg15NH2	Gly367**H**:O{219}	2.74	
Arg15C	Ser344**H**:OG{195}	2.80	Transition state
Arg15O	Gly342**H**:N{193}	2.80	Oxyanion hole
Arg15O	Ser344**H**:N{195}	3.01	Oxyanion hole
Leu17N	Leu177**H**:O{41}	3.15	
His18NE2	His209**H**:O{57}	2.68	
Arg20NH2	Asp196**H**:OD2{60}	2.66	Salt bridge
Tyr34O	Lys341**H**:NZ{192}	3.02	
Leu39N	Gly237**H**:O{97}	2.84	
Glu46OE2	Lys199**H**:NZ{60C}	2.50	Salt bridge

(Figure 4). Comparison with the trypsin·BPTI structure shows that the distal region of 5L15 is rotated slightly (5-6°) around Arg15 in the S1 specificity site, away from the S′ sites toward the S binding sites. Somewhat similar inhibitor movements have been reported in other Kunitz-type inhibitor complexes with trypsin (Perona *et al*., 1993) and thrombin (van de Locht *et al*., 1997).

The (Asp11-Arg15) segment of 5L15, corresponding with P5-P1 sites of substrate, makes an antiparallel β-strand interaction with (Ser363**H**-Gly365**H**){214-216} of VIIa having a hydrogen bond between Pro13O-Gly365**H**:N{216} and a longer one between Arg15N-Ser363**H**:O{214} (Table 2). The carboxylate group of the Asp11 side-chain makes a hydrogen-bonded salt bridge with the side group guanidinium of Arg290**H**{147} that is shared with Lys341**H**:NZ{192} (Figure 4). Both of these interactions are not possible with trypsin or thrombin. In trypsin, residue 147 is a serine and the loop containing it (Thr144-Tyr151) has a conformation different from its equivalent in VIIa, while residue 192 is a glutamine in trypsin and the side-chain hydrogen bonds with Cys14O of BPTI; in thrombin, the equivalent residues are threonine and glutamate, respectively. An Arg147 occurs in Xa, but the P5 position of its natural TFPI-K2 inhibitor is a proline, although the inhibitor does have an aspartate at P6 (Figure 1).

The pyrrolidine of Pro13 of 5L15 makes van der Waals contacts with several residues lining the S3 subsite, Trp364**H**-Gly365**H**{215-216} in particular. The Cys14-Cys38 disulfide bridge at P2 occupies a relatively large apolar S2 subsite, making close contacts with His193**H**{57}, (Gly237**H**-Thr239**H**){97-99} and Ser363**H**{214} (at least one distance <4.0 Å) and fits into the region surprisingly well and collision free. The S1 specificity site of VIIa is filled with the Arg15 side-chain, which extends into an elongated pocket, similar to that of trypsin, thrombin and Xa, where it forms a doubly hydrogen-bonded salt bridge with Asp338**H**{189}. Interactions also occur between Arg15N-Ser344-**H**:OG{195} and Arg15NH2-Gly367**H**:O{219} (Table 2). Binding of 5L15 residues N-terminal to the scissile bond of substrate is completed with the carbonyl oxygen atom of Arg15 making hydrogen bonds with Gly342**H**:N{193} and Ser344**H**:N{195} of the oxyanion hole of VIIa that is also found in other serine proteases. Although there is little electron and positive difference density between Arg15C of 5L15 and Ser344**H**:OG{195} of the catalytic triad of VIIa, the C-OG distance is a short 2.8 Å, suggesting a transition state intermediate-like interaction similar to that observed in the binding of peptidic aldehydes (Krishnan *et al*., 1998) and similar inhibitors (Ganesh *et al*., 1996) with thrombin. The geometry of the scissile bond of the inhibitor, however, is nearly planar (Figure 4), suggesting that the primary binding loop of 5L15 remains intact, as observed in the trypsin·BPTI complex.

The first 5L15 residue comparable with the residue C-terminal to the scissile bond of substrate (P1′) is Ala16. Its methyl group fits into a small confined space defining a S1′ subsite similar to that of thrombin (Matthews *et al*., 1996; St. Charles *et al*., 1999) and makes van der Waals contacts with the side-chains of Cys178**H**{42}, His193**H**{57} of VIIa and more distantly, with Leu177**H**{41}. A hydrogen bond occurs between Leu17N at P2′ and Leu177**H**:O{41} (Table 2), which is also observed in the trypsin·BPTI complex. The side-chain of Leu17 additionally packs against the other side of Gly342**H**{193} and close to the methylene groups of Lys341**H**{192} (Figure 4), and assumes a χ_1 angle optimal for this packing arrangement because of the neighboring bulky phenolic group of Try34. The packing arrangement within this region of the S2′ site was also found in a thrombin-inhibitor complex where a phenethyl group at P1′ extended to the edge of the site (St. Charles *et al*., 1999).

The Ile18His mutation at the P3′ position of 5L15 is unique and appears to be important. The His18NE atom is positioned correctly to make a hydrogen bond with His193**H**:O{57} (2.7 Å, ∠NE-O-C = 154°), which also indicates that His18 is protonated in TF·VIIa·5L15. Of all the natural amino acid residues, only histidine has the correct size, geometry and rotational freedom to achieve such an interaction. Of the four other 5L15-related anticoagulants made by random mutagenesis/phage selection (Stassen *et al*., 1995), two had a His18 along with 0.2 and 5.0 nM binding constants for TF·VIIa. It is indeed impressive that the method leads to the one amino acid at this position that can produce additional direct stabilization in VIIa·5L15 and is found in the mutants of highest affinity. The last mutation (Ile19Leu) in the active site binding segment proved structurally unimportant. The residue is surface exposed in the complex next to Arg20 and does not interact with VIIa (Figure 4).

Several additional polar interactions occur between 5L15 and VIIa in peripheral contact regions bordering the active site of VIIa. Adjacent to the Ile19Leu mutation is Arg20, which forms a

hydrogen-bonded salt bridge with the side-chain of Asp196**H**{60} (Figure 4; Table 2) of a shortened (Asp196**H**-Asn200**H**){60-60D} insertion loop of thrombin (60A-60I). The salt bridge is not found in the trypsin·BPTI complex because trypsin has a lysine at this position. The change of Val34Tyr in 5L15 maintains a mutationally silent hydrogen bond with VIIa (Tyr34O-Lys341**H**:NZ{192}). It is not found in the trypsin·BPTI complex because, as mentioned above, Gln192NE2 of trypsin hydrogen bonds with Cys14O of the inhibitor instead. Little or nothing appears to be gained by the mutation, since the Lys341**H**:NZ{192} can hydrogen bond with the main-chain of any amino acid. As in trypsin·BPTI, Gly36O and all of Gly37 pack against the imidazole of His193**H**{57}. The Arg39Leu mutation and Cys38 of 5L15 make contacts with Gly237**H**-Thr238**H**{97-98} of VIIa with a main-chain hydrogen bond between Leu39 and Gly237**H**{97} (Table 2) in a surface loop bordering the S3 subsite of VIIa. This loop is shifted about 1.4 Å within the active site compared with its position in the TF·VIIa·DFFR complex, presumably due to binding the bulkier 5L15 inhibitor. The loop has a different conformation in the trypsin·BPTI complex and the hydrogen bond is not present; instead, Arg39NE of BPTI makes a close contact to Asn97O (2.9 Å). All of which suggests inherent flexibility in the region.

The final mutation in 5L15, Lys46Glu, is important and leads to the fifth hydrogen-bonded (2.4 Å) salt bridge of VIIa·5L15, interacting with Lys199**H**{60C} of the VIIa insertion loop (Figure 4). The Glu46 residue is found in both TFPI-K1 and TFPI-K2. The lysine side-chain in the TF·VIIa·5L15 complex shows one of the few conformational differences in structure found with respect to TF·VIIa·DFFR. The movement of the lysine appears to simply facilitate the formation of the salt bridge in TF·VIIa·5L15.

The total number of contacts between 5L15 and VIIa < 3.5 Å is 61. Of these, about 30 % are hydrogen bonds of which five are hydrogen-bonded salt bridges (Table 2). This corresponds with about 784 Å^2 of VIIa surface covered by 5L15. In addition, 17 well-defined hydrogen-bonded water molecules form a primary hydration layer around 5L15. Nine of the water molecules make 12 hydrogen bonds with main-chain peptide atoms; the remaining water molecules hydrogen bond with polar side groups of 5L15 and six water molecules make hydrogen bonds bridging both 5L15 and VIIa, two of which are found in the specificity pocket. From this, the tight 0.4 nM binding constant of TF·VIIa·5L15 would seem to have an appreciable polar and electrostatic component.

The Asp11-Arg290**H**{147} salt bridge of TF·VIIa·5L15 is of special interest. Although it is clearly important in stabilizing the VIIa·5L15 complex (Figure 4), it plays an ambivalent role interacting with TFPI. Mutation of Arg290**H**{147} to alanine has no effect on the inhibition of the TF·VIIa complex with free TFPI or TFPI·Xa (Rao & Ruf, 1995). However, the rate of assembly of free TFPI with the mutant TF·VIIa complex is reduced somewhat (twofold), while that of TFPI·Xa remains unaltered. The lack of an alanine effect on inhibition and assembly is not in agreement with the salt bridge in the TF·VIIa·5L15 structure. Since the sequence of the P5-P1′ positions of 5L15 and TFPI-K1 only differs at P1 (Figure 1), the non-participation of Arg290**H**{147} may be related to the way lysine of TFPI-K1 is bound in the specificity site of VIIa. Lysine and arginine have been shown to interact differently with Asp189 of the specificity site of thrombin (Weber *et al*., 1994; St. Charles *et al*., 1999) and in the trypsin·BPTI complex (Huber *et al*., 1974). The lysine binding effect could conceivably propagate a shift to the P5 position that could preclude the formation of a salt bridge with Arg290**H**{147}, thus diminishing the role of the latter in VIIa bound TFPI-K1.

Table 3. Binding constants of different Kunitz-like domains (nM)

	TF·VIIa	Xa	Trypsin
5L15	0.4[a]	52[a]	0.01[a]
TFPI-K1	530[b]/250[c] (120)[d]	[e]	-
TFPI-K2	>90	90 (0.02)[d]	-
BPTI	9800	>9800	0.05

[a] Stassen *et al*. (1995).
[b] Dennis & Lazarus (1994).
[c] Petersen *et al*. (1996).
[d] Binding constant in full-length TFPI.
[e] Does not bind as separate domain.

Seven of the eight mutations of BPTI in 5L15 (Figure 1) improve binding affinity for TF·VIIa by about 25,000-fold and possibly, even that for trypsin (fivefold; Table 3). The 5L15 mutant also has moderate nanomolar affinity for Xa. This contrasts with the individual Kunitz domains of TFPI, which by themselves show considerably reduced affinity (Wesselschmidt *et al*., 1992; Petersen *et al*., 1992, 1996; Higuchi *et al*., 1992; Dennis & Lazarus, 1994; Table 3); however, a recent report questions this (Burgaring *et al*., 1997) but does not resolve the issue. The difference in affinity for TF·VIIa between 5L15 and a separate TFPI-K1 domain is 1300 (Dennis & Lazarus, 1994) or 600 (Petersen *et al*., 1996; Table 3). The only obvious differences in the possible interactions of the two are: (1) in the S1 specificity site (Arg15 in 5L15, Lys15 in K1) and (2) at the S3′ site (Met18His mutation). The Lys15 (Figure 1) accounts for most of the weaker inhibitory activity of K1. A lysine NZ of small molecule inhibitors interacts with the carboxylate of Asp189 of thrombin in two different ways (Weber *et al*., 1995; St. Charles *et al*., 1999), and a third way in the trypsin·BPTI complex (Huber *et al*., 1974), although there is a subtle change in the specificity site of trypsin (Ser190 for Ala190). In any case, none of the three is as efficient as an arginine (Figure 4): the K_i of Ac-D-Phe-Pro-Lys boronate for thrombin is about two orders of magnitude greater than its arginyl analog (Weber *et al*., 1995). If the

same applies to the TFPI-K1 domain and 5L15, the mutation at P1 is the primary reason for the increased binding affinity. The factor of six or thirteen (Table 3) that remains between the two must then be due to the new hydrogen bond that forms between His18 and His193**H**{57} in VIIa·5L15 as the result of the His18 mutation (Figure 4; Table 2).

The fact that TFPI-K2 binds to Xa 4500 times better than a separate K2 domain (Table 3), clearly indicates that other regions of TFPI must be involved in binding (Wesselschmidt *et al*., 1992; Petersen *et al*., 1992, 1996; Higuchi *et al*., 1992), while 5L15 has twice the affinity of a separate K2 domain for Xa (Table 3). This suggested modeling the Xa·TFPI-K2 interaction based on the TF·VIIa·5L15 structure might prove informative. The modeling was done by superposing the VIIa structure of VIIa·5L15 on that of Xa (Padmanabhan *et al*., 1993; rms$\Delta = 0.86$ Å, 214 C^{α} atom pairs) and replacing six different 5L15 residues (Asp11, Pro13, Leu17, His18, Leu19, Tyr34; Figure 1), of 13 in contact regions of Xa (P5-P5′ and residues 34, 39, 46; Ripka *et al*., 1995), with those of TFPI-K2. The resulting model indicated that Pro11 at the P5 position and the Cys14-Cys38 disulfide of K2 collided with the side-chain of Tyr99 of Xa (chymotrypsinogen numbering; Padmanabhan *et al*., 1993). Since Kunitz domains are so highly isostructural, the unacceptable clash around the disulfide suggests a conformational change must take place in Xa, rather than K2, to accommodate binding. The binding of Arg15 in the specificity site and Gly16-Tyr17 (Figure 1) can be the same as VIIa·5L15 (Table 2), except possibly for the encroachment of Gln192 of Xa on the phenolic Tyr17 ring. A significant difference is encountered at the P3′ position of K2 (Figure 1), because the side group of Ile18 cannot form a hydrogen bond like His18 of 5L15. Another major difference between the two complexes is at Arg20, which cannot form a salt bridge in Xa because the equivalent of Asp196**H**{60} of VIIa is Tyr60 in Xa. However, Glu46 is present in both TFPI domains and can make a salt bridge in Xa with Lys62 comparable with Glu46-Lys199**H**{60C} in VIIa·5L15 (Table 2). Lastly, and possibly of considerable significance, the modeling suggests two new salt bridges are possible in Xa·TFPI-K2 that are not between TFPI-K1 or 5L15 and VIIa, which involve Arg32 of K2/Glu37 of Xa and Lys34 of K2/Glu39 of Xa (Figure 1), although replacement of Lys34 by valine improves Xa binding by a factor of 50 (Ripka *et al*., 1995). Most of this is in general agreement with a more detailed modeling analysis based on the structure of the trypsin·TFPI-K2 complex superposed on the structure of Xa (Burgaring *et al*., 1997). Although the independent approaches converged to similar conclusions, it was not possible to resolve the discrepancy of the binding constants ($K_i = 90$ nM, Petersen *et al*., 1996; 0.15 nM, Burgaring *et al*., 1997) from the modeled interactions of either. The two new salt bridges predicted between K2 and Xa would support higher binding affinity for the separate domain, whereas the conformational change required at Tyr99 of Xa, to alleviate close contacts, and the loss of three salt bridges compared to VIIa·5L15 (two at Asp11, one at Arg20; Table 2), can more than offset the positive contributions of the former. Thus, without additional information, arguments are possible in support of both cases.

The EGF1 module

The C-terminal helix of the Gla domain and the first EGF module of VIIa bind a second high-affinity calcium (Schiodt *et al*., 1992), like the corresponding domains of IX (Rao *et al*., 1995) and X (Selander-Sunnerhagen *et al*., 1992). This Ca^{2+} in TF·VIIa·5L15 has full occupancy and $B = 26$ Å^2 with pseudo-octahedral, seven coordination (Table 1). An up-down puckered equatorial plane consists of: Asp46**L**:OD2 and Gly47**L**:O of the C-terminal helix of the Gla domain, both carboxylate oxygen atoms of Asp63**L**, which straddle the plane above and below, and Gln64**L**:O (Figure 3). The apical positions are occupied by Gln49**L**:OE1 and a partially occupied water molecule (O^w455, occupancy 0.7, $B = 28$ Å^2), which is also hydrogen bonded to TF through Gln110**T**:OE1 (3.1 Å). This water molecule was not found in TF·VIIa·DFFR and consequently, neither was its interaction with TF. The Gln110**T** amide nitrogen further hydrogen bonds with Gln64**L**:OE1 in both TF complexes (Figure 3; Table 4), whereas Gln110**T**:NE2 hydrogen bonds with Ser43**L**:OG in TF·VIIa·DFFR but not in the 5L15 complex. The position of the C-terminal helix of the Gla domain is shifted in TF·VIIa·5L15; consequently, Ser43**L**:OG makes a different hydrogen bond to Thr203**T**:OG1 instead (Table 4). Although the former hydrogen bond is probably the physiologically relevant one, the latter indicates that TF and VIIa can also adapt differently. Since the structures of VIIa in TF·VIIa and IXa (Brandstetter *et al*., 1995) and the Gla-domainless structures of Xa (Padmanabhan *et al*., 1993) and protein C (Mather *et al*., 1996) show that EGF2 and the catalytic domain are an intimately connected unit, the functional role of this Ca^{2+} binding site appears to be to fix and maintain the correct relative positions of the Gla and EGF1 domains with respect to one another (Sunnerhagen *et al*., 1996; Kelly *et al*., 1997), restricting overall flexibility to between the EGF modules, for subsequent binding with the TF cofactor. Thus, unlike the catalytic domain Ca^{2+} site, this binding site must make a significant energetic and entropic contribution along with a Ca^{2+}-folded Gla domain to the 0.4 pM TF·VIIa binding constant. The oxygen distances coordinating this high affinity Ca^{2+} ion site are given in Table 1.

The EGF1 module has *O*-glysosylation sites at Ser52**L** and Ser60**L** (Bjoern *et al*., 1991). The first had electron density in TF·VIIa·5L15 that was fitted with glucose, along with about 7-8 Å of additional electron and positive difference density

Table 4. Polar interactions of TF·VIIa

	TF	VIIa	*d* (Å)	Domain
	Lys20**T**:NZ	Cys70**L**:O	2.76	EGF1
	Lys20**T**:NZ	Gly78**L**:O	3.07	EGF1
	Glu24**T**:OE2	Arg79**L**:NH2	3.54	Salt bridge, EGF1
	Ser39**T**:OG	Arg277**H**:NH2{134}	2.78	CAT
	Thr40**T**:O	Arg277**H**:NH2{134}	3.05*	CAT
	Gly43**T**:O	Arg277**H**:NH2{134}	3.27	CAT
	Asp44**T**:OD1	Arg277**H**:N{134}	2.86*	CAT
	Trp45**T**:N	Phe275**H**:O{132}	3.17	CAT
	Lys48**T**:NZ	Glu77**L**:OE1	3.11	Salt bridge, EGF1
TF1	Glu56**T**:OE1	Arg79**L**:NH2	2.76	Salt bridge, EGF1
	Glu56**T**:OE2	Arg79**L**:NE	3.37	Salt bridge[a], EGF1
	Asp58**T**:OD2	Gly78**L**:N	2.53	EGF1
	Asp61**T**:OD2	Lys85**L**:NZ	2.60*	Salt bridge, 1-2 linker
	Glu91**T**:OE1	Thr307**H**:N{165}	2.73*	CAT
	Glu91**T**:OE2	Arg379**H**:NH2{230}	2.62*	Salt bridge, CAT
	Glu91**T**:OE2	Arg379**H**:NH1{230}	2.93*	Salt bridge, CAT
	Tyr94**T**:OH	Asp309**H**:OD2{167}	2.54	CAT
	Tyr94**T**:OH	Asp309**H**:N{167}	3.46	CAT
	Tyr94**T**:O	Gln308**H**:NE2{166}	3.35	CAT
	Asn96**T**:ND2	Asp309**H**:OD1{167}	2.78	CAT
	Gln110**T**:N	Gln64**L**:OE1	2.94	EGF1
	Arg135**T**:NH1	Cys72**L**:O	3.13[b]	EGF1
	Arg135**T**:NH2	Cys72**L**:O	3.40*	EGF1
TF2	Tyr156**T**:OH	Arg36**L**:NH2	2.74[b]	GLA
	Gln190**T**:OE1	Arg36**L**:NH2	2.96[b]	GLA
	Thr203**T**:OG1	Ser43**L**:OG	2.69[b]	GLA
	Asp204**T**:OD1	Arg36**L**:NH1	3.05[b]	Salt bridge, GLA

All the interactions, excluding those of the Gla domain, occur in TF·VIIa·5L15 and TF·VIIa·DFFR; however, those marked with an asterisk were not described by Banner *et al*., (1996).

[a] Not a hydrogen-bonded salt bridge.

[b] Not found in TF·VIIa·DFFR.

meandering into interstitial solvent space. Although the carbohydrate at Ser52**L** is thought to be a mixture di and tri-saccharides (one or two xylose in addition to glucose), this density could not be definitely fitted with sugars, and was not. The Ser60**L** site was readily modeled with its one attached fucose molecule (Bjoern *et al*., 1991).

The TF structure

The structure of TF in the TF·VIIa·5L15 complex is similar to the crystal structures of uncomplexed soluble TF, and is practically identical with that in the TF·VIIa·DFFR structure. Comparisons of the current model of TF in TF·VIIa·5L15 based on an optimal superposition of C^{α} positions were made using coordinates of the different TF structures. All the TF coordinates overlap with a rms difference of less than 1.0 Å, the TF·VIIa·DFFR structure exhibiting the best agreement (rms$\Delta = 0.42$ Å; 176 C^{α} positions), while the high-resolution (1.7 Å) TF-structure (Muller *et al*., 1996) had the largest dissimilarity (rms $\Delta = 0.95$ Å; 180 C^{α} atoms). No significant difference ($\pm 7^{\circ}$) in the interdomain elbow angle ($\sim 125^{\circ}$) is found among the four structures compared, supporting the assertion that the TF molecule is relatively rigid (Martin *et al*., 1995). When comparing the separate domains of the molecule, the N-terminal domain (TF1, Thr6**T**-Asn107**T**), in general, shows less structural variation than the C-terminal membrane proximal domain (TF2, Leu108**T**-Glu210**T**).

The structure of the TF1 domain is nearly complete in TF·VIIa·5L15, only missing a single surface segment between Ala80**T** and Gly90**T**. This region appears to have a penchant for flexibility and disorder, since similar but different length segments are also missing in the other structures of TF. In the case of TF·VIIa·DFFR, the TF was first subjected to limited subtilisin digestion that generated two fragments, (Asn5**T**-Glu84**T**) and (Glu90**T**-Met210**T**), purportedly to facilitate crystal growth (Kirchhofer *et al*., 1995).

Interactions between TF and VIIa

The TF·VIIa interaction surface runs nearly the entire length of the TF molecule (Figure 2). The catalytic and EGF1 domains of VIIa together participate in over three-quarters of the interaction surface between VIIa and TF. The total accessible surface area buried on binding VIIa by TF in the TF·VIIa·5L15 complex is 1667 Å^2, somewhat less than that observed in the TF·VIIa·DFFR complex (1881 Å^2) due to the missing N-terminal Gla domain segment of the former. The 784 Å^2 of VIIa covered by 5L15 compares well with that of TF·VIIa. This is especially so for the number of contacts <3.5 Å (61 for VIIa·5L15; 79 for TF·VIIa), which is about twice as efficient (contacts/buried surface) for VIIa·5L15. Except for the Gla domain helix of the light chain, interactions between TF and VIIa are generally conserved in the 5L15 and DFFR inhibited structures of TF·VIIa. A list of the

polar interactions is presented in Table 4. The TF1 domain contributes over 73% of the accessible surface buried between TF and VIIa in the TF·VIIa·5L15 complex, and interacts with several segments of the enzyme, mostly from the EGF1 and catalytic domains of VIIa.

The (Ser39**T** -Tyr51**T**) segment of TF1 interacts with (Phe275**H**-Phe278**H**){132-135} and (Met306**H**-Leu309**H**){164-167} of the catalytic domain, as well as a short segment of EGF2 (Glu77**L**, (Val92**L**-Glu94**L**)). The N-terminal 39-45 stretch interacts with (Phe275**H**-Phe278**H**){132-135) and forms a shallow hydrophobic pocket in which the arginyl group of Arg277**H**{134} resides, interacting mostly with Ser39**T**, Asp44**T** and Trp45**T**. This loop undergoes a significant shift compared with the same region in uncomplexed TF structures. The Arg277**H**{134} has been implicated in cofactor affinity by alanine scanning mutagenesis (Dickinson *et al*., 1996). The Asp44**T** residue, which makes a hydrogen bond with Arg277**H**{134} (Table 4), has been shown by mutagenesis to be involved in the enhancement and regulation of VIIa catalytic function (Kelly *et al*., 1996). Although charge neutralization by asparagine replacement did not reduce TF function, replacement by alanine resulted in a mutant with eightfold reduced affinity for binding VIIa. Furthermore, VIIa amidolytic function by the TF-Ala44 mutant was reduced 25% relative to wild-type, and proteolytic function was diminished sixfold. All of these results indicate that the Arg277**H**{134} hydrogen bond interaction is significantly enhancing proteolysis of macromolecular substrate by VIIa.

Residues (Glu91**T**-Asn96**T**) form an intercalating hydrophobic surface that associates with a complementary surface of the catalytic domain made of side-chains from Met306**H**{164}, Glu308**H**{166}, Asp309**H**{167} and Arg379**H**{230} (Table 4). The side-chain of Tyr94**T** packs closely against that of Met306**H**{164}, which forms the inner wall of an apolar cavity into which the tyrosyl group inserts. The Arg277**H**{134}, Met306**H**{164) and Asp309**H**{167} interactions have been shown to affect cofactor affinity (Dickinson *et al*., 1996). Active site occupancy additionally affects cofactor binding, enhancing the affinity for TF by essentially decreasing the dissociation rate of the TF·VIIa complex. Of the three residues, only Met306**H**{164} played a major role in inhibitor induced increase of binding affinity.

A VII variant with a serine substitution at Phe328**H**{181} (VII central) has been identified in a severe VII deficiency (Bharadwaj *et al*., 1996). The variant exhibited <1% VII procoagulant activity, a twofold decrease in affinity for TF and did not activate IX or X in the presence of TF after activation by Xa. In addition, VIIa central showed no amidolytic activity in the presence of TF. Homology modeling of the VIIa central protease domain based on the structure of Xa and molecular dynamics simulations (Bharadwaj *et al*., 1996) suggested that the striking inability of Phe328**H**{181}Ser VIIa to cleave substrates may be due to the formation of a new hydrogen bond between Tyr377**H**{228} and the all-important Asp338**H**{189} of the S1 specificity site. The Phe328**H**{181} residue in TF·VIIa·5L15 is located near the center of a highly hydrophobic cavity, buried among the side-chains of His348**H**{199}, Tyr377**H**{228}, the methylene groups of Arg304**H**{162} and Arg379**H**{230}, the methyl group of Ala330**H**{183} and the main-chain segment (Tyr377**H**-Arg379**H**){228-230}. Furthermore, Phe328**H**{181} is about 12 Å from the carboxylate group of Asp338**H**{189} and 6 Å from that of Glu91**T**. Replacement of the Phe328**H**{181} residue in its highly hydrophobic environment by a polar serine would be expected to disturb the region. Thus, the decrease in TF affinity of VIIa central is most likely related to the disruption of the salt bridge between Glu91**T** and Arg379**H**{230} (Table 4). The drastic catalytic differences of the single Phe328**H**{181}Ser VIIa mutation must also be due to the structural reorganization of the hydrophobic cavity, although it is more difficult to rationalize from only the wild-type structure.

In summary, the interactions described here between TF, the two EGF modules and the catalytic domain of VIIa in TF·VIIa·5L15 all occur in the TF·VIIa·DFFR structure as well, although some were not discussed in describing the latter (Table 4). Another reassuring observation is that the limited subtilisin proteolysis of TF in TF·VIIa·DFFR (Kirchhofer *et al*., 1995) does not affect the overall folding and quaternary structure of TF or the manner in which the cleaved cofactor binds with VIIa.

The Gla domain of TF·VIIa·5L15

The $(2F_o - F_c)$ and $(F_o - F_c)$ electron density in the region of the Gla domain was incomplete and not well defined, particularly in the early stages of the work. The C-terminal α-helix of the domain containing a characteristic stacked Phe40**L**, Trp41**L**, Tyr44**L** aromatic triplet (Seshadri *et al*., 1991; Soriano-Garcia *et al*., 1992) was resolved, but the density still terminated at Arg36**L**. Further refinement failed to reveal any more structure of the domain. Since the concentration of Ca^{2+} in the crystallization mother liquor was 1.5 mM or less (see Materials and Methods), it is conceivable that the N-terminal 35 residues of the domain are not folded into a tertiary structure and are flexibly and/or statically disordered in the crystals. Such was the case with the structure of apo-prothrombin fragment 1 where the N-terminal 35 residues of the Gla domain were confirmed to be disordered in the absence of Ca^{2+} ion by virtue of N-terminal sequencing of crystalline material (Seshadri *et al*., 1991). Conversely, however, it is also conceivable that the N-terminal 32 or so residues of VIIa have been proteolyzed by VIIa itself. Precedence for the latter has been set by the report of the removal of the Gla domain of VIIa at Lys32**L** by VIIa in the

absence of Ca^{2+} incubated for 24 hours at 37°C (Sabharwal *et al*., 1995). Considering that: (1) the concentration of Ca^{2+} was most likely less than 1.5 mM, about half the binding constant of the high affinity Ca^{2+} sites of the Gla domain; (2) the VIIa was only reversibly, not covalently inhibited; and (3) the crystallization of the TF·VIIa·5L15 complex generally took place over a period of about a week, a des-Gla domain TF·VIIa·5L15 complex in the crystals with a disordered (Asp33**L**-Gla35**L**) N-terminal tripeptide was also a likely possibility. This led us to measure the MALDI-MS spectra of VIIa and crystalline material that confirmed the proteolysis.

The interactions between the C-terminal half of TF2 and the truncated Gla domain are unique to the TF·VIIa·5L15 complex (Table 4), because of a substantial repositioning of the C-terminal Gla domain helix (Arg36**L**-Ser45**L**). Although the helix packs against the inner aspect of TF2 as in the TF·VIIa·DFFR complex, the N terminus of it is pivoted by approximately 33deg from the membrane binding region of TF2, toward the interdomain hinge region (Figure 2). Moreover, the solvent-accessible side of the helix packs closely against an EGF1 module of a symmetry related molecule, creating an environment that clearly does not have enough space to harbor a folded Gla domain based on volume considerations of the Gla domain in Ca^{2+} prothrombin fragment1 (Soriano-Garcia *et al*., 1992) and in the TF·VIIa·DFFR structure. The tight intermolecular contact may be at least partially responsible for the repositioning of the helix. However, the region N-terminal to the helix opens to a large solvent cavity, which is also close to the disordered loops of the membrane proximal region of TF2. The region is spacious enough to accommodate an unfolded 35 residue chain of the Gla domain. When the EGF2 and catalytic domains are superposed with those of TF·VIIa·DFFR (rmsΔ remains 0.35 Å), the C^{α} positions of the EGF1 structures begin to diverge near Ala75**L** and exhibit a maximal shift of about 2.2 Å near Gly47**L**, close to the Gla-EGF1 Ca^{2+} binding site, in a direction apparently drawing the EGF1 of the TF·VIIa·5L15 closer to TF2. When the EGF2 and catalytic domains are optimally superposed, the rmsΔ between the EGF1 modules of TF·VIIa·5L15 and TF·VIIa·DFFR is 1.5 Å, while the rmsΔ = 0.51 Å when the EGF1 modules of the two complexes are superposed alone. The helix repositioning may represent a low energy packing arrangement favored in the absence of the intact folded Gla domain revealing an unexpected degree of adaptability.

In the TF·VIIa·DFFR complex, the Gla domain interacts with TF2 primarily through hydrophobic contacts between Trp158**T**, Val207**T**, the Cys186**T**-Cys209**T** disulfide bridge in TF, and Phe31**L**, Phe40**L** of the Gla domain. These contacts are, for the most part, missing in the TF·VIIa·5L15 complex. Instead, at least four new polar interactions are observed as a consequence of the helix repositioning (Table 4), none of which are found in the TF·VIIa·DFFR complex. The OG1 atom of Thr203**T** makes a hydrogen bond with Ser43**L**:OG due to a relative translation of the helix in an N-terminal direction. More significantly, the side-chain of Arg36**L**, which occupies an apolar region adjacent to Trp158**T** in the TF·VIIa·DFFR complex, is directed toward a solvent-accessible area of TF2 in TF·VIIa·5L15 and makes a hydrogen bond with Gln190**T**:OE1 and a hydrogen-bonded salt bridge with Asp204**T**:OD1. A hydrogen bond also occurs between Arg36**L**:NH2 and the hydroxyl oxygen of Tyr156**T**. Thus, much of the movement of the helix may be the result of satisfying the Arg36**L** interactions. In contrast with the TF·VIIa·DFFR complex, only Phe40**L** participates in hydrophobic interactions with TF2: the side-chain is located in a region occupied by the side-chain of Leu39**L** in the TF·VIIa·DFFR structure and it makes hydrophobic contacts with the side groups of Asp204**T** and Val207**T**.

Comparison of the structures of VIIa and IXa

The only other crystal structure of a full-length multi-domain blood coagulation proteinase reported thus far is that of hemophilia B-related IXa at 3.0 Å resolution (Brandstetter *et al*., 1995)†. The IXa, inhibited irreversibly with D-Phe-Pro-Arg chloromethyl ketone, was crystallized in the absence of Ca^{2+}, so the 30-35 N-terminal residues of the Gla domain were not folded and were flexibly disordered as in apo-prothrombin fragment 1 (Seshadri *et al*., 1991). There was, however, a cylindrical electron density feature corresponding to the C-terminal helix of the domain, which formed the basis for modeling the remainder of the Gla domain in its folded calcium bound state using the structure of Ca^{2+}-prothrombin fragment 1 (Soriano-Garcia *et al*., 1992). We have compared here the full-length structure of VIIa in TF·VIIa·DFFR (Banner *et al*., 1996) with that of IXa. The rms difference in the superposition of 221 C^{α} coordinates of the catalytic domains of VIIa and IXa is 1.1 Å. Although the EGF2 modules of both enzymes also superimpose similarly, the Gla-EGF1 tandem of IXa is oriented about right angles to that of VIIa (Figure 5). The principal axes of the EGF modules in VIIa are nearly in line with one another, whereas they make an angle of about 110° in IXa stabilized by a salt bridge between two conserved residues in IXa (Glu78 and Arg95; Brandstetter *et al*., 1995)‡. Although Glu78 is also

† The structures of Gla-domainless Xa (Padmanabhan *et al*., 1993) and the anticoagulant enzyme activated protein C (Mather *et al*., 1996), which have three domains homologous to VIIa and IXa, have been determined at 2.2 and 2.8 Å resolution, respectively.

‡ The angle between the EGF domains of activated protein C is similar at 80° (Mather *et al*., 1996); the EGF1 domain is disordered in Xa (Padmanabhan *et al*., 1993).

Figure 5. Stereoview of the superposition of the C^{α} positions of the EGF2 and catalytic domain of VIIa of TF·VIIa·DFFR on the corresponding domains of IXa. VIIa in continuous lines, IXa broken lines.

conserved in VIIa, Xa and protein C, Arg95 is not, so that the salt bridge is truly unique to IXa. The different domain orientations between VIIa and those of IXa could arise in several different ways. One is through a conformational change in VIIa on binding to TF thus accounting for its dramatic increase in catalytic efficiency (Osterud & Rapaport, 1977; Silverberg *et al*., 1977). The different orientations could also come about from crystal packing effects in IXa, since the molecular structures of the two TF·VIIa complexes are practically the same but the crystal packing arrangements are different ($C222_1$ for TF·VIIa·5L15; $P2_12_12_1$ for TF·VIIa·DFFR). Another possibility is simply that considerable mobility may generally exist between the domains because intact multi-domain blood proteins have not been easy to crystallize. That IXa did crystallize could be related to the dimeric-like IXa units in the crystal structure, the inter-dimer interactions of which might stabilize and fix the structure of the full-length molecule. Other full-length, multi-domain blood protease structures could resolve the anomaly, if in fact one actually exists.

Materials and Methods

Crystallization

The VIIa used for crystallization was a kind gift from Dr Walter Kisiel (University of New Mexico) in the form of a frozen solution of 0.83 mg/ml VIIa in 50 mM Tris-HCl (pH 7.5), 2 mM $CaCl_2$. A tenfold molar excess of lyophilized 5L15 (Corvas International, San Diego, CA) dissolved in a 20 mM Tris-HCl (pH 7.4), 50 mM NaCl, 2 mM $CaCl_2$ buffer solution was placed over a thawing VIIa aliquot to inhibit the enzyme. The freshly inhibited enzyme was allowed to stand at room temperature for 15 minutes; it was then stored at 4 °C for about 15 hours. The TF complex of VIIa·5L15 was made by adding a 10 % molar excess of TF (3.1 mg/ml in 20 mM Tris-HCl (pH 7.5), 0.02 % (w/v) NaN_3), a gift of Dr Thomas J. Girard (Monsanto/Searle Co., St Louis, MO), to the solution of 5L15 inhibited VIIa. The ternary complex thus formed was allowed to stand overnight at 4 °C. The solution of the complex was concentrated using a 50,000 molecular mass cut-off centricon filter in a refrigerated centrifuge. It was then diluted tenfold with buffer and concentrated, three times in all (1000-fold total dilution), in order to remove excess 5L15 and TF. The final concentration of the TF·VIIa·5L15 solution was 13.5 mg/ml in VIIa.

The best crystals of the ternary complex grew by the hanging drop method at room temperature from drops composed of two parts buffer (as above), one part protein solution and one part well solution (0.1 M Na citrate (pH 5.6), 16.0-16.5 % (w/v) PEG4000, 12 % (v/v) 1-propanol) suspended over 600 µl of well solution. This gives a drop with a composition of 3.4 mg/ml in VIIa as a ternary complex in 15 mM Tris-HCl, 25 mM Na citrate, 37.5 mM NaCl, 1.5 mM $CaCl_2$, 4 % (w/v) PEG 4000, 3 % (v/v) 1-propanol. Crystal platelets usually appeared in two to three days, and finished growing within ten days (up to 1.0 mm in length). The crystal used for intensity data collection had dimensions of 0.08 mm × 0.50 mm × 0.70 mm.

Data collection

X-ray diffraction intensities of the TF·VIIa·5L15 complex were measured to 2.0 Å resolution with a Siemens 2 K single chip CCD detector on the Industrial Macromolecular Crystallography Association (IMCA) beamline (17-ID) at the Advanced Photon Source of Argonne National Laboratory. The crystal was briefly transferred to a cryo-protectant solution (100 mM Na citrate (pH 5.6), 20 % (w/v) PEG4000, 20 % (v/v) glycerol) then mounted and flash-frozen at 100 K. The crystal detector distance was 12.0 cm for the intensity measurements at a CCD swing angle of $2\theta = 20°$. Exposures were one second per 0.25 deg. frames with a total of 632 images being recorded. The raw data (166,318 reflections) were integrated and scaled using the SAINT processing program to produce 70,671 unique reflections (average redundancy of 2.35) with a R_{sym}= 0.094 (R_{sym}= $\Sigma|I - \langle I\rangle|/\Sigma I$, where I is the intensity of a reflection and $\langle I\rangle$ is the mean value). The R_{sym} values of the reflections between 2.1-2.0 Å resolution were generally much larger than 30 %, had a smaller redundancy factor and had intensities bordering expected error, so these 9462 reflections were discarded giving a total of 61,209 reflections at 2.1 Å resolution (87 % completion, 78 % completion in the 2.2-2.1 Å range). Of these, 6557 were zero reflections leaving 54,652 unique reflections for structure analysis. The orthorhombic crystals of TF·VIIa·5L15 belong to space group $C222_1$, with unit cell dimensions of $a = 63.49$ Å, $b = 190.0$ Å, $c = 175.3$ Å, eight ternary complexes per unit cell, one complex per asymmetric unit. This gives a Matthews number of 3.68 and a protein fraction of 36 % for a complex with a fully intact Gla domain.

Structure analysis

The structure of the TF·VIIa complex was solved by molecular replacement with the program AMoRe (Navaza, 1994). The catalytic domain of Xa (Padmanabhan *et al*., 1993) and the structure of TF (Muller *et al*., 1994) were used as search models for the TF·VIIa complex. In the search for VIIa, with data in the 10.0-3.5 Å resolution range, an outstanding peak of 15.8 σ was generated. A translation search with this solution produced a peak of 11.9 σ with a crystallographic $R = 50$ %. Following rigid-body refinement, the R-factor was 49 % and the correlation coefficient 0.47. The rotation search for TF was carried out similarly, but in the 15.0-4.0 Å range. No outstanding solutions were identified so translation searches were carried out on the ten highest rotation peaks, also including the position and rotation of the catalytic domain of VIIa in calculations. The sixth highest peak proved to be the correct solution based on crystal packing considerations (peak height 43.8σ, next highest 39.0σ). Rigid-body refinement reduced R to 47 % with a correlation coefficient of 0.54.

Initial positional and simulated annealing refinements were carried out using the program X-PLOR version 3.1 (Brunger, 1993) against 9.0-2.8 Å data. One round of simulated annealing using the slow-cool procedure (2000 K to 300 K in steps of 25 K) followed by several cycles of standard positional refinement reduced the R-factor to 0.37 (R-free = 0.41). The $(2F_o - F_c)$ and (Fo-Fc) difference electron density maps clearly revealed structure for most of the two EGF domains of the VIIa light chain, as well as a large fraction of the 5L15 molecule. The portion of the inhibitor bound at the active site was particularly well defined. These and all other interpretable regions of the structure were modeled

Table 5. Summary of refinement parameters and statistics of TF·VIIa·5L15

Parameters		RMS standard deviations	
Range (Å)	(9.0-2.1)	Bond distance (Å)	0.022 (0.02)[b]
No. reflections	50,314	Bond angle (deg.)	1.3[c]
No. protein atoms	4717	$\langle B \rangle_{prot}$ (Å^2)	27.6
No. water molecules	340[a]	RMS-B_{mc} (Å^2)[d]	1.4[c]
No. variables	20,728	RMS-B_{sc} (Å^2)[d]	3.8[c]
R-value (%)	23.7	$\langle B \rangle_{wat}$ (Å^2)	23.6

[a] Water with occupancy >0.5 only.
[b] Target deviation from ideal value in parenthesis.
[c] The rmsΔ from average value.
[d] The rmsΔ of *B*-factor of bonded atoms (mc, main-chain; sc, side-chain).

using the molecular graphics program CHAIN running on a Silicon Graphics Indigo 2 workstation. A second round of simulated annealing and positional refinement extending data to 2.1 Å resolution ($R = 0.29$; R-free $= 0.34$) improved regions in the maps corresponding to the C-terminal helix of both the Gla domain of VIIa and the 5L15 inhibitor molecule permitting those elements of the structure to be modeled. The resulting coordinates were then subjected to further refinement with the program PROLSQ (Hendrickson, 1985). Individual isotropic temperature factors were constrained not to exceed 50 Å^2 during the course of refinement. The structure was subjected to a number of rounds of manual model rebuilding, each round followed by positional and *B*-factor refinement using a variable, resolution-dependent weighting scheme for the diffraction data. During the final stages of refinement, two calcium ions, two sugar molecules and solvent water molecules were added to the model. The occupancies and temperature factors of the water molecules and calcium ions were refined in an alternating series of refinement cycles (occupancies first, *B* values held constant followed by the reverse). The final structure contains coordinates for 4717 non-hydrogen protein/carbohydrate atoms corresponding with 683 residues of the ternary complex, two calcium ions, and 340 water molecules, giving a final *R*-factor of 0.237 for the 9.0-2.1 Å data. Stereochemical parameters and refinement statistics of the final structure are given in Table 5.

Protein Data Bank accession number

The coordinates of TF·VIIa·5L15 have been deposited in the Brookhaven Protein Data Bank (PDB code: 1FAK).

Acknowledgments

E.Z and R.S.C. contributed equally to the work. This work was supported by NIH Grants HL 25942 and HL 43229. We would like to thank Walt Kisiel (University of New Mexico) and Tom Girard (Monsanto/Searle Co., St Louis, MO) for providing us with abundant quantities of highly purified VIIa and TF, respectively, and for many informative discussions throughout this work. We are grateful to Corvas International Ltd. (San Diego, CA) for their gift of the 5L15 inhibitor and to Dr Terry Brunck thereof for his numerous discussions about the work, and Dr Wolfram Ruf (Scripps Research Insitute) for useful comments about the manuscript. We would also like to thank Scott Warder (University of Notre Dame) for the MALDI-MS measurements.

References

Bajaj, S. P., Sabharwal, A. K., Gorka, J. & Birktoft, J. J. (1992). Antibody-probed conformational transitions in the protease domain of human factor IX upon calcium binding and zymogen activation. *Proc. Natl Acad. Sci. USA*, **89**, 152-156.

Banner, D. W., D'Arcy, A., Chene, C., Winkler, F. K., Guha, A., Konigsberg, W. H., Nemerson, Y. & Kirchhofer, D. (1996). The crystal structure of the complex of blood coagulation factor VIIa with soluble tissue factor. *Nature*, **380**, 41-46.

Baron, M., Main, A. L., Driscoll, P. C., Mardon, H. J., Boyd, J. E. & Campbell, I. D. (1992). H^1 NMR assignment and secondary structure of the cell adhesion type III module of fibronectin. *Biochemistry*, **31**, 2068-2073.

Bharadwaj, D., Iino, M., Kontoyianni, M., Smith, K. J., Foster, D. C. & Kisiel, W. (1996). Factor VII Central. *J. Biol. Chem.* **271**, 30685-30691.

Bjoern, S., Foster, D. C., Thim, L., Wiberg, F. C., Christensen, M., Komiyama, Y., Pedersen, A. & Kisiel, W. (1991). Human plasma and recombinant factor VII. Characterization of *O*-glycosylations at serine residues 52 and 60 and effects of site-directed mutagenesis on serine 52 to alanine. *J. Biol. Chem.* **266**, 11051-11057.

Bode, W. & Schwager, P. (1975). The refined crystal structure of bovine β-trypsin at 1.8 Å resolution. *J. Mol. Biol.* **98**, 693-717.

Bode, W., Turk, D. & Karshikov, A. (1992). The refined 1.9-Å X-ray crystal structure of D-Phe-Pro-Arg chloromethylketone-inhibited human α-thrombin: structure analysis, overall structure, electrostatic properties, detailed active-site geometry, and structure-function relationships. *Protein Sci.*, 1426-1471.

Brandstetter, H., Bauer, M., Huber, R., Lollar, P. & Bode, W. (1995). X-ray structure of clotting factor IXa: active site and module structure related to Xase activity and hemophilia B. *Proc. Natl Acad. Sci. USA*, **92**, 9796-9800.

Broze, G. J., Jr, Girard, T. J. & Novotny, W. F. (1990). Regulation of coagulation by a multivalent Kunitz-type inhibitor. *Biochemistry*, **29**, 7539-7546.

Brunger, A. T. (1993). A system for X-ray crystallography and NMR. In *X-PLOR Manual Version 3.1*, Yale University, New Haven, CT.

Burgaring, M. J. M., Orbons, L. P. M., van der Doelen, A., Mulders, J., Theunissen, H. J. M., Grootenhuis, P. D. J., Bode, W., Huber, R. & Stubbs, M. T. (1997). The second Kunitz domain of human tissue factor inhibitor. *J. Mol. Biol.* **269**, 395-407.

Davie, E. W., Fujikawa, K. & Kisiel, W. (1991). The coagulation cascade: initiation, maintenance, and regulation. *Biochemistry*, **30**, 10363-10370.

Dennis, M. S. & Lazarus, R. A. (1994). Kunitz domain inhibitors of tissue factor-Factor VIIa. *J. Biol. Chem.* **269**, 22137-22144.

Dickinson, C. D., Kelly, C. R. & Ruf, W. (1996). Identification of surface residues mediating tissue factor binding and catalytic function of the serine protease factor VIIa. *Proc. Natl Acad. Sci. USA*, **93**, 14379-14384.

Fisher, K. L., Gorman, C. M., Vehar, G. A., O'Brien, D. P. & Lawn, R. M. (1987). Cloning and expression of human tissue factor cDNA. *Thrombosis Res.* **48**, 89-99.

Ganesh, V., Lee, A. Y., Clardy, J. & Tulinsky, A. (1996). Comparison of the structures of cyclotheonamide A complexes of human α-thrombin and β-bovine trypsin. *Protein Sci.* **5**, 825-835.

Hardy, J. F. & Desroches, J. (1992). Natural and synthetic anti-fibrinolytics in cardiac surgery. *Can. J. Cardiol.* **39**, 353-365.

Harlos, K., Martin, D. M. A., O'Brien, D. P., Jones, E. Y., Stuart, D. I., Pollkarpov, I., Miller, A., Tuddenham, E. G. D. & Boys, C. W. G. (1994). Crystal structure of the extracellular region of human tissue factor. *Nature*, **370**, 662-666.

Hendrickson, W. A. (1985). Stereochemically restrained refinement of macromolecular structure. *Methods Enzymol.* **115**, 252-270.

Higuchi, D. A., Wun, T. C., Likert, K. M. & Broze, G. J., Jr (1992). The effect of leukocyte elastase on tissue factor pathway inhibitor. *Blood*, **79**, 1712-1719.

Huang, M., Syed, R., Stura, E. A., Stone, M. J., Stefanko, R. S., Ruf, W., Edgington, T. S. & Wilson, I. A. (1998). The mechanism of an inhibitory antibody on TF-initiated blood coagulation revealed by the crystal structures of human tissue factor, Fab 5G9 and TF·5G9 complex. *J. Mol. Biol.* **275**, 873-894.

Huber, R., Kukla, D., Bode, W., Schwager, P., Bartels, K., Deisenhofer, J. & Steigemann, W. (1974). Structure of the complex formed by bovine trypsin and bovine pancreatic trypsin inhibitor. *J. Mol. Biol.* **89**, 73-101.

Ichinose, A. & Davie, E. W. (1994). The blood coagulation factors. In *Hemostasis and Thrombosis: Basic Principles and Clinical Practice* (Colman, R. W., Hirsch, J., Marder, V. J. & Salzman, E. W., eds), 3rd edit., pp. 19-54, J. B. Lippincott Co., Philadelphia, PA.

Kelly, C. R., Schullek, J. R., Ruf, W. & Edgington, T. S. (1996). Tissue factor residue Asp44 regulates catalytic function of the bound proteinase factor VIIa. *Biochem. J.* **315**, 145-151.

Kelly, C. R., Dickinson, C. D. & Ruf, W. (1997). Ca^{+2} binding to the first epidermal growth factor module of coagulation factor VIIa is important for cofactor interaction and proteolytic function. *J. Biol. Chem.* **272**, 17467-17472.

Kirchhofer, D., Guha, A., Nemerson, Y., Konigsberg, W. H., Vilbois, F., Chene, C., Banner, D. W. & D'Arcy, A. (1995). Activation of blood coagulation factor VIIa with cleaved tissue factor extracellular domain and crystallization of the active complex. *Proteins: Struct. Funct. Genet.* **22**, 419-425.

Krishnan, R., Zhang, E., Hakansson, K., Arni, R. K., Tulinsky, A., Lim-Wilby, M. S. L., Levy, O. D., Semple, J. E. & Brunck, T. K. (1998). Highly selective mechanism-based thrombin inhibitors: structures of thrombin and trypsin inhibited with rigid peptidyl aldehydes. *Biochemistry*, **37**, 12094-12103.

Leahy, D. J., Hendrickson, W. A., Aukhil, I. & Erickson, H. P. (1992). Structure of a fibronectin type III domain from tenascin phased by MAD analysis of the selenomethionyl protein. *Science*, **258**, 987-991.

Martin, D. M. A., Boys, C. W. G. & Ruf, W. (1995). Tissue factor: molecular recognition and cofactor function. *FASEB J.* **9**, 852-859.

Mather, T., Oganessyan, V., Hof, P., Huber, R., Foundling, S., Esmon, C. & Bode, W. (1996). The 2.8 Å crystal structure of Gla-domainless activated protein C. *EMBO J.* **15**, 6822-6831.

Matthews, J. H., Krishnan, R., Costanzo, M. J., Maryanoff, B. E. & Tulinsky, A. (1996). Crystal structures of thrombin with thiazole-containing inhibitors: probes of the S1′ binding site. *Biophys. J.* **71**, 2830-2839.

Morrissey, J. H., Fakhrai, H. & Edgington, T. S. (1987). Molecular cloning of the cDNA for tissue factor, the cellular receptor for the initiation of the coagulation protease cascade. *Cell*, **50**, 129-135.

Muller, Y. A., Ultsch, M. H., Kelley, R. F. & de Vos, A. M. (1994). Structure of the extracellular domain of human tissue factor: location of the factor VIIa binding site. *Biochemistry*, **33**, 10864-10870.

Muller, Y. A., Ultsch, M. H. & de Vos, A. M. (1996). The crystal structure of the extracellular domain of human tissue factor refined to 1.7 Å resolution. *J. Mol. Biol.* **256**, 144-159.

Navaza, J. (1994). AMoRe: an automated package for molecular replacement. *Acta Crystallog. sect. A*, **50**, 157-163.

Nemerson, Y. (1988). Tissue factor and hemostasis. *Blood*, **71**, 1-8.

Orthner, C. L. & Kosow, D. P. (1978). The effect of metal ions on the amidolytic activity of human factor Xa. *Arch. Biochem. Biophys.* **185**, 400-406.

Orthner, C. L. & Kosow, D. P. (1980). Evidence that human α-thrombin is a monovalent cation-activated enzyme. *Arch. Biochem. Biophys.* **202**, 63-75.

Osterud, B. & Rapaport, S. I. (1977). Activation of factor IX by the reaction product of tissue factor and factor VII: additional pathway for initiating blood coagulation. *Proc. Natl Acad. Sci. USA*, **74**, 5260-5264.

Padmanabhan, K., Padmanabhan, K. P., Tulinsky, A., Park, C. H., Bode, W., Huber, R., Blankenship, D. T., Cardin, A. D. & Kisiel, W. (1993). Structure of human des (1-45) factor Xa at 2.2 Å resolution. *J. Mol. Biol.* **232**, 947-966.

Perona, J. J., Tsu, C., Craik, C. S. & Fletterick, R. J. (1993). Crystal structures of rat anionic trypsin complexed with the protein inhibitors APPI and BPTI. *J. Mol. Biol.* **230**, 919-933.

Persson, E., Hogg, P. J. & Stenflo, J. (1993). Effects of Ca^{+2} binding on the protease module of factor Xa and its interaction with factor Va. *J. Biol. Chem.* **268**, 22531-22539.

Petersen, L. C., Bjorn, S. E. & Nordfang, O. (1992). Effect of leukocyte proteinases on tissue factor pathway inhibitor. *Thrombosis Haemostasis*, **67**, 537-541.

Petersen, L. C., Bjorn, S. E., Olsen, O. H., Nordfang, O., Norris, F. & Norris, K. (1996). Inhibitory properties of separate recombinant Kunitz-type-protease-inhibitor domains from tissue-factor-pathway-inhibitor. *Eur. J. Biochem.* **235**, 310-316.

Rao, L. V. M. & Rapaport, S. I. (1988). Activation of factor VII bound to tissue factor: a key early step in

the tissue factor pathway of blood coagulation. *Proc. Natl Acad. Sci. USA*, **85**, 6687-6691.

Rao, L. V. M. & Ruf, W. (1995). Tissue factor residues Lys165 and Lys166 are essential for rapid formation of the quaternary complex of tissue factor·VIIa with Xa·tissue factor pathway inhibitor. *Biochemistry*, **34**, 10867-10871.

Rao, Z., Handford, P., Mayhew, M., Knott, V., Brownlee, G. G. & Stuart, D. (1995). The structure of a Ca^{+2}-binding epidermal growth factor-like domain: its role in protein-protein interactions. *Cell*, **82**, 131-141.

Rapaport, S. (1989). Inhibition of factor VIIa/tissue factor-induced blood coagulation with particular emphasis upon a factor Xa-dependent inhibitory mechanism. *Blood*, **73**, 359-365.

Ripka, W., Brunck, T., Stanssens, P., LaRoche, Y., Lauwereys, M., Lambeir, A-M., Lasters, I., De Maeyer, M., Vlasuk, G., Levy, O., Miller, T., Webb, T., Tamura, S. & Pearson, D. (1995). Strategies in the design of inhibitors of serine proteases of the coagulation cascade: factor Xa. *Eur. J. Med. Chem.* **30**, 87-100.

Sabharwal, A. K., Birktoft, J. J., Gorka, J., Wildgoose, P., Petersen, L. C. & Bajaj, S. P. (1995). High affinity Ca^{+2}-binding site in the serine protease domain of human factor VIIa and its role in tissue factor binding and development of catalytic activity. *J. Biol. Chem.* **270**, 15523-15530.

Scarpati, E. M., Wen, D., Broze, G. J., Miletich, J. P., Flandermeyer, R. R., Siegel, N. R. & Sadler, J. E. (1987). Human tissue factor: cDNA sequence and chromosome localization of the gene. *Biochemistry*, **26**, 5234-5238.

Schiodt, J., Harrit, N., Christensen, U. & Petersen, L. C. (1992). Two different Ca^{+2} ion binding sites in factor VIIa and in des(1-38) factor VIIa. *FEBS Letters*, **306**, 265-268.

Selander-Sunnerhagen, M., Ullner, M., Persson, E., Teleman, O., Stenflo, J. & Drakenberg, T. (1992). How an epidermal growth factor (EGF)-like domain binds calcium. *J. Biol. Chem.* **267**, 19642-19649.

Seshadri, T. P., Tulinsky, A., Skrzypczak-Jankun, E. & Park, C. H. (1991). Structure of bovine prothrombin fragment 1 refined at 2.25 Å resolution. *J. Mol. Biol.* **220**, 481-494.

Silverberg, S. A., Nemerson, Y. & Zur, M. (1977). Kinetics of the activation of bovine coagulation factor X by components of the extrinsic pathway. *J. Biol. Chem.* **252**, 8481-8488.

Soriano-Garcia, M., Padmanabhan, K., de Vos, A. M. & Tulinsky, A. (1992). The Ca^{+2} ion and membrane binding structure of the Gla domain of Ca^{+2}-prothrombin fragment 1. *Biochemistry*, **31**, 2554-2566.

Spicer, E. K., Horton, P., Bloem, L., Bach, R., Williams, K. R., Guha, A., Kraus, J., Lin, T. C., Nemerson, Y. & Konigsberg, W. H. (1987). Isolation of cDNA clones coding for human tissue factor: primary structure of the protein and cDNA. *Proc. Natl Acad. Sci. USA*, **84**, 5148-5152.

Stassen, J. M., Lambeir, A-M., Matthyssens, G., Ripka, W. C., Nystrom, A., Sixma, J. J. & Vermylen, J. (1995). Characterization of a novel series of aprotinin-derived anticoagulants. *Thrombosis Haemostasis*, **74**, 646-654.

St. Charles, R. S., Matthews, J. H., Zhang, E. & Tulinsky, A. (1999). The bound structures of novel P3-P1′ β-strand mimetic inhibitors of thrombin. *J. Med. Chem.* in the press.

Steiner, S. A. & Castellino, F. J. (1982). Kinetic studies of the role of monovalent cations in amidolytic activity of activated bovine plasma protein C. *Biochemistry*, **21**, 4609-4614.

Strickland, D. K. & Castellino, F. J. (1980). The binding of calcium to bovine factor VII. *Arch. Biochem. Biophys.* **190**, 687-692.

Stura, E. A., Wilson, L. A. & Ruf, W. (1996). Crystallization and preliminary crystallographic data for a ternary complex between tissue factor, factor VIIa and a BPTI-derived inhibitor. *J. Crystal Growth.* **168**, 260-269.

Sunnerhagen, M., Olah, G. A., Stenflo, J., Forsen, S., Drakenberg, T. & Trewhella, J. (1996). The relative orientation of Gla and EGF domains in coagulation factor X is altered by Ca^{+2} binding to the first EGF domain. *Biochemistry*, **35**, 11547-11559.

van de Locht, A., Bode, W., Huber, R., Le, Bonniec B. F., Stone, S. R., Esmon, C. T. & Stubbs, M. T. (1997). The thrombin E192Q:BPTI complex reveals gross structural rearrangements. *EMBO J.* **16**, 2977-2984.

Verstraete, M. (1985). Clinical application of inhibitors of fibrinolysis. *Drugs*, **29**, 236-261.

Weber, P. C., Lee, S.-L., Lewandowski, F. A., Schadt, M. C., Chang, C.-H. & Kettner, C. A. (1995). Kinetic and crystallographic studies of thrombin with Ac-(D)Phe-Pro-boroArg-OH and its lysine, amidine, homolysine and ornithine analogs. *Biochemistry*, **34**, 3750-3757.

Wells, C. M. & DiCera, E. (1992). Thrombin is a Na^{+}-activated enzyme. *Biochemistry*, **31**, 11721-11730.

Wesselschmidt, R., Likert, K., Girard, T. J., Wun, T. C. & Broze, G. J., Jr. (1992). Tissue factor pathway inhibitor: the carboxy-terminus is required for optimal inhibition of factor Xa. *Blood*, **79**, 2004-2010.

Zhang, E. & Tulinsky, A. (1997). The molecular environment of the Na^{+} binding site of thrombin. *Biophys. Chem.* **63**, 185-200.

Edited by R. Huber

(Received 7 September 1998; received in revised form 26 November 1998; accepted 30 November 1998)